

See discussions, stats, and author profiles for this publication at: <https://www.researchgate.net/publication/41396652>

Interfacial Reactions of Ozone with Surfactant Protein B in a Model Lung Surfactant System

ARTICLE in JOURNAL OF THE AMERICAN CHEMICAL SOCIETY · FEBRUARY 2010

Impact Factor: 12.11 · DOI: 10.1021/ja908477w · Source: PubMed

CITATIONS

19

READS

28

10 AUTHORS, INCLUDING:



Young Shik Shin

NanoIVD, Inc

29 PUBLICATIONS 1,912 CITATIONS

SEE PROFILE



Evan L Neidholdt

California Institute of Technology

13 PUBLICATIONS 59 CITATIONS

SEE PROFILE



William A. Goddard

California Institute of Technology

1,350 PUBLICATIONS 69,703 CITATIONS

SEE PROFILE

Published in final edited form as:

J Am Chem Soc. 2010 February 24; 132(7): 2254–2263. doi:10.1021/ja908477w.

Interfacial Reactions of Ozone with Surfactant Protein B in a Model Lung Surfactant System

Hugh I. Kim^a, Hyungjun Kim^{b,†}, Young Shik Shin^c, Luther W. Beegle^a, Seung Soon Jang^d, Evan L. Neidholdt^c, William A. Goddard^b, James R. Heath^c, Isik Kanik^a, and J. L. Beauchamp^{c,*}

^a Jet Propulsion Laboratory, California Institute of Technology, Pasadena, CA 91109

^b Materials and Process Simulation Center, Beckman Institute, California Institute of Technology, Pasadena, CA 91125

^c Noyes Laboratory of Chemical Physics, California Institute of Technology, Pasadena, CA 91125

^d School of Materials Science and Engineering, Georgia Institute of Technology, Atlanta, GA 30332-0245

Abstract

Oxidative stresses from irritants such as hydrogen peroxide and ozone (O₃) can cause dysfunction of the pulmonary surfactant (PS) layer in the human lung, resulting in chronic diseases of the respiratory tract. For identification of structural changes of pulmonary surfactant protein B due to the heterogeneous reaction with O₃, field induced droplet ionization (FIDI) mass spectrometry is utilized. FIDI is a soft ionization method in which ions are extracted from the surface of microliter-volume droplets. We report the structurally specific oxidative changes of SP-B₁₋₂₅ (a shortened version of human surfactant protein B) at the air-liquid interface. We also present studies of the interfacial oxidation of SP-B₁₋₂₅ in a non-ionizable 1-palmitoyl-2-oleoyl-*sn*-glycerol (POG) surfactant layer as a model PS system, where the competitive oxidation of the two components is observed. Our results indicate that the heterogeneous reaction of SP-B₁₋₂₅ at the interface is quite different from that in the solution phase. Compared to the nearly complete homogeneous oxidation of SP-B₁₋₂₅, only a subset of the amino acids known to react with ozone is oxidized by direct ozonolysis in the hydrophobic interfacial environment, both with and without the lipid monolayer. Combining these experimental observations with the results of molecular dynamics simulations provides an improved understanding of the interfacial structure and chemistry of a model lung surfactant system when subject to oxidative stress.

Introduction

The cardiopulmonary system is constantly exposed to airborne environmental hazards. Long-term and immediate exposure of the lungs to pathogens, air pollutants, and other irritants can be a major cause of acute and chronic injuries such as cardiopulmonary mortality and lung cancer.^{1–4} Lung disease is the third leading cause of death in the United States; approximately \$154 billion is spent for direct and indirect lung disease-related health care every year.⁴ Recently, Jerret et al. studied the effect of the tropospheric ozone on the risk of death from any

*To whom correspondence should be addressed: jlbchamp@caltech.edu.

[†]Current Address: Graduate School of EEWS, Korea Advanced Institute of Science and Technology, Daejeon 305-701, Republic of Korea

Supporting Information Available: Additional figures and complete Ref. ³⁵. This material is available free of charge via the Internet at <http://pubs.acs.org>.

cause and cause-specific in a large cohort of the United States. They reported a significant increase in the risk of death from respiratory causes in association with an increase in ozone (O₃) concentration on air pollution.¹ Lung disease death rates are still increasing and more efforts to understand the chemical as well as the physical characteristics of lung system are required.

Pulmonary surfactant (PS) is a mixture of lipids and proteins found in the lungs that reduces the surface tension of the alveolar sacs during the breath cycle.⁵ Phospholipids form oriented monolayers at the air-liquid interface achieving a very low surface tension (~0 mN/m)^{6,7} to ease the adsorption and spreading of the air-liquid interface in the lung alveolar sacs.⁷ Surfactant protein B (SP-B) enhances phospholipid adsorption and spreading from the sub-phase to the interface,^{6,8,9} and inherited deficiencies in SP-B are lethal at birth.^{8,10} Despite its vital importance, little is known about the interactions of this protein with phospholipid in the PS. Furthermore, the detailed chemical change of major components has not been studied thoroughly when the PS is exposed to oxidants such as O₃.

A number of studies have reported the chemical changes of major components of PS under various oxidative stresses,^{11–13} as well as changes in physical properties, which cause acute lung injury and respiratory failure.^{2,14,15} For example, Uppu et al. used human red-blood cell membranes as a model lung system and demonstrated their oxidation *via* a solution phase O₃ application.¹² Yet, understanding detailed mechanisms of chemical and physical changes of the PS system at the air-liquid interface is still an active and challenging field of research. In particular, the oxidative change of major PS components by a heterogeneous air-liquid reaction with an external oxidative source (i.e. O₃) has not been studied thoroughly at the molecular level. Air-liquid heterogeneous chemistry of atmospherically relevant molecules has been studied thoroughly using mass spectrometric,^{16–18} spectroscopic,^{19–22} and surface tensiometric techniques,^{23,24} along with theoretical methods.^{25,26} Fewer studies have considered the air-liquid interfacial chemistry of biologically relevant systems. Exemplifying the latter, Colussi and co-workers recently reported heterogeneous reactions with O₃ of ascorbic acid²⁷ and uric acid²⁸, which are components of the pulmonary epithelial lining fluid, using mass spectrometry.

Field-induced droplet ionization mass spectrometry (FIDI-MS) comprises a soft ionization method to sample ions from the surface of microliter droplets.^{16,29,30} A pulsed electric field stretches neutral droplets until they develop dual Taylor cones, emitting streams of positively and negatively charged submicron droplets in opposite directions. A quiescent hanging droplet is formed on the end of a capillary and then exposed to gas-phase reactants for a variable period of time, followed by FIDI-MS sampling of molecular species present in the interfacial layer (Figure 1).

In this study, we utilize FIDI-MS for probing air-liquid interfacial oxidation of SP-B₁₋₂₅ (FPIPLPYCWLCRALIKRIQAMIPKG) by O₃. SP-B₁₋₂₅, comprising the 25 N-terminal amino acids of wild type SP-B, mimics the lung activities of the full length protein.^{9,31,32} The structural features of SP-B₁₋₂₅ include predominant α -helical structure (residues 8 - 22), N-terminal (residues 1 - 6) β sheet conformation, and C-terminal (residues 23 - 25) random structure.³³ We sample the droplet containing SP-B₁₋₂₅ exposed to a constant flux of O₃ gas over a range of reaction times to analyze distinct air-liquid interfacial chemistry. Then, we investigate the difference between the interfacial and solution phase reactions of O₃ with SP-B₁₋₂₅. Oxidation using the Fenton reaction is also performed to compare the solution phase ozonolysis to solution phase oxidation by OH radical. Finally, we investigate the heterogeneous reaction of a model PS system composed of SP-B₁₋₂₅ and 1-palmitoyl-2-oleoyl-*sn*-glycerol (POG) with O₃. POG is non-ionizable lipid and used to avoid undesired competition of ionization with SP-B₁₋₂₅ at the surface of the droplet during the FIDI experiment. Structures

of POG, and SP-B₁₋₂₅ are shown in Scheme 1. To more fully interpret on experimental observations, positioning of SP-B₁₋₂₅ in a lipid monolayer is examined using molecular dynamic (MD) simulations.

Experimental

Chemicals and Reagents

Ammonium bicarbonate (NH₄HCO₃), iron(II) dichloride (FeCl₂), sodium ethylenediaminetetraacetic acid (EDTA), trypsin from porcine pancreas were purchased from Sigma-Aldrich (St. Louis, MO). SP-B₁₋₂₅ was purchased from Biomer Technology (Hayward, CA). Sodium salts of POG were purchased from Avanti Polar Lipid (Alabaster, AL). All solvents (hydrogen peroxide, water, methanol, acetic acid) were purchased from EMD Chemicals Inc. (Gibbstown, NJ).

Online FIDI-MS Technique and Heterogeneous Oxidation by O₃

The FIDI-MS instrument used in this investigation were based on designs previously described by Grimm et al.¹⁶ A ~2 mm o.d. droplet of analyte solution is suspended from the end of a 28-gauge stainless steel capillary (Small Parts Inc.), which is located between the atmospheric sampling inlet of a ThermoFinnigan LCQ Deca mass spectrometer and a parallel plate electrode. The droplet is located on center in the region between the plate electrode and the MS inlet; the plate and inlet were separated by 6 mm. The O₃ outlet is located 1 mm from the droplet in order to reduce mechanical perturbation of the droplet by the flow of O₃. Ozonolysis reactions occur between 0 and 30 s after a quiescent droplet is achieved (~1 – 2 s). Then, a high-voltage pulse is applied on the parallel plate electrode and sampling capillary. The high-voltage pulse establishes a field of $\pm 7 \times 10^5$ V m⁻¹, 20 ms duration to achieve FIDI. This is just above the threshold required for FIDI to be observed. A pencil-style UV calibration lamp (model 6035, Oriel) generates ~20 ppm O₃, measured spectrophotometrically using an absorption cell with 10 cm path length and calculated with Beer's Law using an the molar absorption coefficient of 1.15×10^{-17} cm² molecule⁻¹, in air that continually washes through the FIDI region at 1500 mL min⁻¹. Because of its high toxicity, the ozone level in the laboratory was monitored using Ozone Test Strips (OzoneLab, Canada) and all experimentalists used particulate filter masks (3M, St. Paul, MN) for personal protection during the experiment. 50 μM SP-B₁₋₂₅, or a mixture of 100 μM POG and 50 μM SP-B₁₋₂₅ in 1:1 (by volume) water and methanol feed the droplet source. A previous study of the secondary structure of SP-B₁₋₂₅ reports that the peptide conserves predominate α-helical conformation in aqueous, lipid, and alcohol environments.³³ We assume that the peptide preserves α-helical structure in either a water-methanol mixture or a POG monolayer. The negative or positive 4 kV and 2 kV, 20 ms pulses to the plate electrode and capillary respectively initiate FIDI and direct charged progeny into the LCQ for mass analysis in positive (SP-B₁₋₂₅) mode. The FIDI-MS spectra reported in this study were obtained by averaging five to ten individually acquired spectra from separately prepared droplets. The nomenclature proposed by Roepstorff and Fohlman³⁴ is used for the parent and fragment ions.

Solution Phase O₃ Reaction

A continuous flow of ~20 ppm O₃ in air was applied to the 100 μM SP-B₁₋₂₅ solution in 1:1 (by volume) water and methanol solvent for 30 s, 1, 1.5, 2, 3, 4, and 5 min. The SP-B₁₋₂₅ solution was diluted to 50 μM for ESI with 1:1 water/methanol and 1% acetic acid by volume. Product analysis was performed on a Micromass QTof2 quadrupole time of flight mass spectrometer in the positive ion mode. Trypsin digests of SP-B₁₋₂₅ and O₃ treated SP-B₁₋₂₅ were prepared by incubating 200 μM of SP-B₁₋₂₅ with 6 μg of trypsin from porcine pancreas in 1 mL of water containing 25 mM ammonium bicarbonate (NH₄HCO₃) at 37 °C for 4 hours. The trypsin was then removed using a Millipore Microcon centrifugal filter fitted with an

Ultracel YM-10 membrane. The sample solution was diluted to an appropriate concentration for ESI with 1:1 water/methanol and 1% acetic acid by volume. Product analysis was performed on a Thermo Finnigan LCQ Deca XP ion trap mass spectrometer (ITMS) in positive and negative modes.

Fenton reaction

SP-B₁₋₂₅ (500 μ M) was incubated with 600 μ M FeCl₂, 600 μ M sodium EDTA, and 30 mM H₂O₂ in 1 mL water at 37 °C for 12, 18, and 24 h. The peptide was purified using a Varian C₁₈ OMIX 100 μ L pipette tip. The sample solution was diluted to an appropriate concentration with 1:1 water/methanol and 1% acetic acid by volume. Product analysis was performed on a Micromass QToF2 quadrupole time of flight mass spectrometer in the positive ion mode.

Molecular Dynamic Simulations

The MD simulations were performed with the all-atom CHARMM PARAM27³⁵ force field using the LAMMPS (Large-scale Atomic/Molecular Massively Parallel Simulator) code.³⁶ To describe the water, we used a flexible TIP3P potential, which needs additional Hooke's constants, K of 900 kcal/mol/Å² for OH bond and K of 110 kcal/mol/rad² for HOH angle to the 3-site-rigid TIP3P model.³⁵ The initial conformation of SP-B₁₋₂₅ was taken from the Protein Data Bank structure (1DFW). The particle-particle particle-mesh method³⁷ was employed to compute the electrostatic interactions using an accuracy criterion of 10⁻⁴.

The initial structures for the lipid monolayer-water systems were prepared with 48 hexagonally-packed lipids on the 3168, 3264, 3744, and 4464 water molecules for the 55, 60, 65, and 70 Å²/Lipid surface densities, respectively. A pure-repulsive wall potential, $E = \epsilon[2/15 (\sigma/r)^9 - (\sigma/r)^3]$, where $\epsilon = 0.1521$ kcal/mol and $\sigma = 3.1538$ Å with cut-off distance of 2.7071 Å, was applied at $z = 0$ to prevent the water from diffusing in the negative z -direction. The dimensions of the simulation cells used were (55.21 \times 47.82 \times 200.0 Å) for the 55 Å²/Lipid, (57.67 \times 49.94 \times 200.0 Å) for the 60 Å²/Lipid, (60.02 \times 51.98 \times 200.0 Å), for the 65 Å²/Lipid, and (62.28 \times 53.94 \times 200.0 Å) for the 70 Å²/Lipid surface densities. The systems were equilibrated for 0.5 ns using 300 K NVT MD simulations by applying Nose-Hoover thermostat with a temperature damping relaxation time of 0.1 ps. Then, 2.0 ns NVT MD simulations were performed, and these trajectories are employed for the analysis of the atomic profiles.

The initial structure for the SP-B₁₋₂₅ in the POG or 1-palmitoyl-2-oleoyl-phosphatidylglycerol (POPG) monolayer was constructed using the final structure after the simulation of the lipid monolayer-water system with the surface density of 60 Å². After removing six neighboring lipids, the SP-B₁₋₂₅ is inserted into the resultant cavity with an α -helical axis orientation angle of 34° to the interfacial plane. Then the dimensions of the simulation cells were slightly adjusted to (57.88 \times 50.12 \times 200.0 Å). Similar to the lipid monolayer simulations, 0.5 ns equilibration followed by 2.0 ns NVT MD simulation was performed at 300 K. To analyze the trajectories, we averaged the population over the last 0.5 ns of the 2.0 ns trajectories. In order to consider effects of only the waters near the interface, the oxygen atoms with $\Delta z > -15$ Å were included in analyzing the xy-projected populations of the water.

Results and Discussion

Interfacial Oxidation of SP-B₁₋₂₅

The positive ion FIDI-MS spectrum of SP-B₁₋₂₅ is shown in Figure 2 (top). The doubly protonated SP-B₁₋₂₅ is observed as the dominant species in the FIDI-MS spectrum before O₃ application. As discussed earlier, FIDI-MS samples ions from the surface of the droplet.¹⁶ SP-B₁₋₂₅ contains four cationic amino acid (AA) residues, which are Arg₁₂, Lys₁₆, Arg₁₇, and Lys₂₄ (Scheme 1). The peptide exhibits amphiphilic characteristics with the hydrophobic N-

terminal side and the hydrophilic C-terminal side. The hydrophobic N-terminal side of the peptide is expected to project above the air-liquid interface, while the hydrophilic C-terminal side remains solvated at the interface. In contrast to the other strongly basic AA residues, Arg₁₂ is located between Leu₁₀ and Leu₁₄ in the hydrophobic portion of the peptide (Scheme 1). We suggest that the observed doubly charged SP-B₁₋₂₅ likely results from protonation of Lys₂₄ and Arg₁₇ in the solvated hydrophilic portion of the peptide. Protonation of Lys₁₆ is not as likely due to coulomb repulsion with the adjacent cationic arginine.

The time resolved oxidation of SP-B₁₋₂₅ by O₃ is monitored using FIDI-MS (Figure 2). Products resulting from the oxidation of SP-B₁₋₂₅ by O₃ appear after the droplet is exposed to O₃ for 5 s. The products at m/z 1481 and m/z 1489 correspond to doubly protonated SP-B₁₋₂₅ with two oxygen atoms and with three oxygen atoms, respectively. The FIDI-MS spectrum of the droplet with SP-B₁₋₂₅ is dominated by the triply oxygenated product at m/z 1489 after exposing the droplet to O₃ for 10 s. No further oxidation of the peptide is observed up to 30 s of exposure. The FIDI-MS spectra imply that the doubly oxygenated product immediately undergoes further oxidation to form the stable product with three oxygen atoms.

Solution Phase Oxidation of SP-B₁₋₂₅

In order to investigate the difference between the interfacial and solution phase reactions of O₃ with SP-B₁₋₂₅, O₃ was bubbled into a solution containing SP-B₁₋₂₅. Oxidation using the Fenton reaction is also performed to compare the solution phase ozonolysis to solution phase oxidation by OH radical. For the comparison to heterogeneous ozonolysis of SP-B₁₋₂₅, the products with three additional oxygen atoms from both reactions are analyzed.

In contrast to the FIDI-MS spectrum, triply and quadruply protonated SP-B₁₋₂₅ are observed as the dominant ions in the ESI-MS spectrum, with a smaller amount of the doubly protonated peptide (Figure 3a). No significant oxygenated product is observed when applying O₃ for 30 sec or less to the peptide solution. However, after 1 min of O₃ application, incorporation of three and nine oxygens in SP-B₁₋₂₅ are observed as major products. Other less abundant oxygenated peptides (+4 O and +5 O) are also observed as minor products in the spectrum. No further oxidized product was observed after applying O₃ for 5 min. Figure 3b shows oxidized products of SP-B₁₋₂₅ after applying O₃ for 3 min to the SP-B₁₋₂₅ solution, with the predominant 3- and 9- oxygenated SP-B₁₋₂₅ products indicated in the spectrum. The relative abundance of 9-oxygenated SP-B₁₋₂₅ compared to 3-oxygenated peptide increases as the charge state of the ions decreases. It is suggested that the more completely oxidized species does not yield an abundant +4 charge state ion since oxidized residues such as cysteic acids form salt bridges with basic AA residues (i.e. Arg and Lys) of the peptide. The oxidized products of triply and quadruply charged SP-B₁₋₂₅ from the Fenton reaction with intact SP-B₁₋₂₅ are shown in Figure S1 in Supporting Information. The Fenton reaction yields a series of oxidized SP-B₁₋₂₅ products with up to 10 oxygen atoms.

Structure Analysis of Extensively Oxidized SP-B₁₋₂₅ from Solution Phase Ozonolysis

In order to determine structures of the oxidized SP-B₁₋₂₅ formed by the solution phase O₃ reaction, a trypsin digest was performed after applying O₃ for 3 min to the SP-B₁₋₂₅ solution. The ESI mass spectrum of a trypsin digest of SP-B₁₋₂₅ exhibits 7 major ion peaks. The masses and segments of the observed tryptic digest ions of SP-B₁₋₂₅ are indicated in Figure 4a. The ESI mass spectrum of a trypsin digest of SP-B₁₋₂₅ oxidized by reaction with solution phase O₃ exhibits segments with MetSO (m/z 817, m/z 874, and m/z 1030) and the less abundant N-terminal segment of FPIPLPYCWLCR + 80 at m/z 1636 in positive ion mode (Figure 4b). The negative ion mode ESI mass spectrum also exhibits corresponding deprotonated segment ion peaks (Figure 4c).

The structures of segments are confirmed by collision induced dissociation (CID) spectra. As seen in Figure 5a, the CID of the ion at m/z 817 exhibits the elimination of hydrosulfinylmethane (CH_4SO , 64 mass unit), which is the characteristic dissociation pathway of methionine sulfoxide (MetSO).^{38,39} The structure of the segment FPIPLPYCWLCR + 8O is also investigated using CID. Fragments from the CID of the cationic FPIPLPYCWLCR + 8O at m/z 1636 yields y -type fragments (y_7 and y_9) with all eight oxygen atoms as dominant products (Figure 5b). The fragment PLPYCW with six oxygen atoms indicates that Cys₈ and Trp₉ are oxidized to sulfonic acid (+3O) and hydroxy-N-formylkynurenine (HNFKyn, +3O, Scheme 2), respectively. The structures are further confirmed by the fragments of $c_8+3\text{O}$ and PLPYC+3O resulting from the CID of FPIPLPYCWLCR + 8O in negative ion mode (Figure 5c). The extra two oxygen atoms are assigned to Cys₁₁ (+2O). It is notable that Cys₈ and Cys₁₁ are located in close proximity to each other in the helical structure.³² The fact that we do not observe formation of sulfonic acid for both of the closely located Cys residues is possibly caused by the formation of sulfonic anhydride ($\text{R}_1\text{-O}_2\text{SOSO}_2\text{-R}_2$). No significant segment peak is observed from a triply oxygenated SP-B₁₋₂₅ after tryptic digest of the products from the solution phase O_3 reaction.

Comparative Structure Analysis of 3-Oxygenated SP-B₁₋₂₅ from Solution and Interfacial Ozonolysis

In comparison to the more extensive solution phase oxidation of SP-B₁₋₂₅, the interfacial reaction results in the addition of only 3 oxygen atoms to the protein fragment. It is of interest to compare the structures of the 3-oxygenated product from both reactions using CID. The FIDI-CID spectrum (FIDI-MS²) of the triply oxygenated SP-B₁₋₂₅ product at m/z 1489 from heterogeneous oxidation is shown in Figure 6a. CID yields an exclusive fragment at m/z 1457 resulting from the elimination of CH_4SO . This indicates that the oxidation of the methionine residue (Met₂₁) in SP-B₁₋₂₅ results from the heterogeneous ozonolysis. The other two oxygen atoms are added to the tryptophan residue (Trp₉) forming NFKyn (Scheme 2).

Figures 6b and 6c show CID spectra (ESI-MS²) of triply oxygenated products of quadruply protonated SP-B₁₋₂₅ from solution phase O_3 application and from the Fenton reaction, respectively. The ESI-MS² spectrum of the triply oxygenated SP-B₁₋₂₅ by solution phase O_3 application implies the presence of two products, one with NFKyn (+2O) and MetSO (+1O), and the other with HNFKyn (+3O) (Figure 6b). Evidence of the MetSO in the oxidized SP-B₁₋₂₅ is found from the CID experiment involving the quadruply charged SP-B₁₋₂₅ product from the solution phase O_3 reaction. For example, the paired fragments of $y_{20}\text{-CH}_4\text{SO}$ and y_{20} fragments, which are observed at m/z 782 and m/z 803 (triply charged) and at m/z 1172 and m/z 1204 (doubly charged), confirm the presence of MetSO (Figure 6b). Interesting CID fragments are also observed in the ESI-MS² spectrum. The singly charged fragment at m/z 680, m/z 832, and m/z 938 are WLCRA+3O, LPYCWLCRALIKR+3O and PLPYCWLCRALIKRI+3O, respectively. These fragments are evidence of the formation of HNFKyn through the oxidation of Trp₉ from the solution phase O_3 reaction. This is further supported by the singly charged fragment at m/z 652, QAMIPK-NH₃, which indicates that no oxidation has occurred at Met₂₁. The ESI-MS² spectrum of the triply oxygenated SP-B₁₋₂₅ by solution phase O_3 reaction implies the presence of two products, one with NFKyn (+2O) and MetSO (+1O), and the other with HNFKyn (+3O). The CID fragment abundance implies that the solution phase O_3 reaction with SP-B₁₋₂₅ yields more product peptides with HNFKyn compared to product peptides with NFKyn and MetSO. The ESI-MS² spectrum of SP-B₁₋₂₅ product from the Fenton reaction is shown in Figure 6c. The CID of the Fenton product exhibits the presence of HNFKyn at m/z 652, m/z 680, and m/z 938, which correspond to the singly charged fragments QAMIPK-NH₃, WLCRA+3O, and PLPYCWLCRALIKRI+3O, respectively. However, evidence for the formation of the product with NFKyn and MetSO is not found in the spectrum.

Unique Features of the Interfacial Reaction of SP-B₁₋₂₅ with O₃

Ozone has limited solubility in water. For a gas-phase concentration of 20 ppm O₃, the equilibrium concentration of O₃ dissolved in aqueous solution is calculated as 22.6 nM by Henry's law.⁴⁰ In addition, O₃ is unstable in water, and rapidly forms secondary reactive oxygen species (ROS).⁴¹ The major secondary ROS formed by O₃ in water is OH radical.⁴² This implies that two major O₃ oxidation pathways, involving ozonolysis and reaction with OH radical, can be observed at the air-liquid interface. The triply oxygenated SP-B₁₋₂₅ is formed concomitantly with the formation of the doubly oxygenated SP-B₁₋₂₅ after exposing the droplet to O₃ for 5 – 10 s (Figure 2). The oxidation mechanisms of Trp, Met, and Cys in peptide are shown in Scheme 2. The NFKyn can be formed via direct ozonolysis of Trp⁴³ or hydrolysis of hydroxytryptophan (HTrp).¹³ However, the formation of MetSO from Met occurs primarily by secondary oxidants.⁴⁴ The NFKyn of the heterogeneous reaction results from the direct ozonolysis of Trp₉, which is located at the hydrophobic N-terminal side of SP-B₁₋₂₅. Met₂₁, which likely forms MetSO, is located at the hydrophilic C-terminal site. Intact Cys₈ and Cys₁₁ support this observed O₃ oxidation of SP-B₁₋₂₅. The reactivity of Cys with ozone in solution phase exceeds that of Trp and Met by two orders of magnitude.⁴⁵ However, the oxidation of Cys to yield cysteinesulfonic acid (CysSO₃H) occurs primarily by reactions with secondary oxidants,⁴⁶ which formed only in the presence of an aqueous environment. This suggests that the hydrophobic N-terminal side of the SP-B₁₋₂₅, where Cys₈ and Cys₁₁ are located, is above the air-liquid interface, while the hydrophilic C-terminal side is immersed in the aqueous layer below the interface. The difference between the solution phase O₃ application and the heterogeneous ozonolysis is clearly observed from the CID of triply oxygenated SP-B₁₋₂₅ (Figure 6). The formation of HNFkyn requires at least one secondary oxidation step (Scheme 2). After NFKyn is formed by either direct ozonolysis or reaction with secondary oxidants, the Met and NFKyn undergo competitive oxidation to yield MetSO ($k = 1.4 \times 10^{-11} \text{ cm}^3 \text{ molecule}^{-1} \text{ s}^{-1}$) and HNFkyn ($k = 1.3 \times 10^{-11} \text{ cm}^3 \text{ molecule}^{-1} \text{ s}^{-1}$) by secondary ROS in the solution phase.⁴⁷

The observed high abundance of SP-B₁₋₂₅ where three and nine oxygen atoms have been added from solution phase ozonolysis can be also explained by the distinct oxidation mechanisms of O₃ in aqueous solution (Figure 3b). The interfacial reactions leading to oxidation of Trp₉ and Met₂₁ to form NFKyn and MetSO by ozonolysis and secondary ROS, respectively, render the peptide more hydrophilic. Decrease of the signal to noise (S/N) ratio of 3-oxygenated SP-B₁₋₂₅ in the FIDI-MS spectra (Figure 2) with extensive ozonolysis suggests that this hydrophilic product dissolves to the bulk liquid. This causes NFKyn, Cys₈, and Cys₁₁ to be exposed to secondary ROS for further oxidation. As a result, NFKyn reacts with secondary ROS to form HNFkyn and, simultaneously, Cys₈ and Cys₁₁ are also oxidized by secondary ROS to form sulfonic anhydride.

Oxidation of SP-B₁₋₂₅ in a POG Surfactant Layer by O₃

The interfacial reaction of SP-B₁₋₂₅ with ozone was also examined in the presence of the neutral lipid POG, which forms a surfactant layer at the air-liquid interface. Almost identical FIDI-MS spectra are observed compared to the spectra obtained for interfacial ozonolysis of SP-B₁₋₂₅ without POG except for a ~5 s time delay for initiation of the reaction (Figure 7). The FIDI-MS spectrum of the SP-B₁₋₂₅/POG droplet is dominated by the triply oxygenated product after 15 s of exposure. No further oxidation of the peptide is observed up to 30 s exposure. The observed ozonolysis products and time delay of the reaction provide critical clues regarding the location and orientation of SP-B₁₋₂₅ in the monolayer.

Kinetics of the heterogeneous ozonolysis of unsaturated phospholipids have been studied previously by several research groups.^{24,48,49} Unsaturated phospholipid disappears at the interface by ozonolysis through the formation of a primary ozonide. Under the assumption that

the O₃ concentration is constant ($\sim 5 \times 10^{14}$ molecule cm⁻³) during the reaction, we can estimate the reaction time using the pseudo-first order rate constant $k_2 = k_1[\text{O}_3]$, where $k_1 = 4.5 \times 10^{-16}$ cm³ molecule⁻¹ s⁻¹ adopted from the 1-oleoyl-2-palmitoyl-sn-glycero-3-phosphocholine (OPPC) ozonolysis on NaCl.⁴⁸ The reaction rate is expressed as

$$-\frac{d[\text{POG}]_{\text{surf}}}{dt} = k_2[\text{POG}]_{\text{surf},0} \quad (1)$$

The time for consuming 90% – 99% of unsaturated lipid to form the POZ at the air-liquid interface is calculated to be $\sim 10 - 20$ s. Both POG and OPPC possess a palmitic acid chain and an oleic acid chain, the latter of which reacts with O₃. Under the assumption that the reactivity of POG is similar to that of OPPC, the initiation of the SP-B₁₋₂₅ ozonolysis is expected after the droplet is exposed to O₃ for 10 – 20 s, if the peptide is completely shielded by lipid acyl chains. However, the observed short time delay of the initiation of SP-B₁₋₂₅ ozonolysis suggests that the peptide competes directly with POG for reaction with O₃. This suggests a picture in which the peptide is colocated at the air-liquid interface with POG at the surface of the droplet. In addition, the ozonolysis of SP-B₁₋₂₅ in the POG monolayer yields identical products compared to the ozonolysis of the peptide alone at the air-liquid interface. This supports the conjecture that SP-B₁₋₂₅ by itself forms an oriented interfacial aggregate or layer at the surface of the droplet. The generally hydrophobic N-terminal portion appears to be packed together in a region depleted of water at the surface of the droplet.

Interactions of SP-B₁₋₂₅ in a Lipid Monolayer

We carried out MD simulations for the POG monolayer in a water box for 2.0 ns with four different surface densities (55, 60, 65, and 70 Å²/lipid), which are reported as a reasonable density range for pulmonary surfactant function from previous theoretical studies.^{50–52} All four surface densities exhibit similar characteristic behavior (Figure S2 in Supporting Information). Then, we performed 2.0 ns duration MD simulations of the POG/SP-B₁₋₂₅/water monolayer with 60 Å²/lipid surface density as a representative case. The final snapshot in Figure 8a shows that the SP-B₁₋₂₅ is located at the air-liquid interface. The hydrophobicity index of each AA residue in the peptide is shown in Figure 8b (top).⁵³ Relatively strong hydrophobicity is found for the N-terminal side of the peptide with Leu, Ile, and Pro residues. In contrast, hydrophilicity is expected from C-terminal side due to Arg, Lys, and Gln residues. The MD simulated $\Delta z_{\text{C}\alpha}$ exhibits a good correlation with the hydrophobicity index. The hydrophobic N-terminal side of the peptide is located above the air-liquid interface ($\Delta z \sim 0$), while the hydrophilic C-terminal side is located inside or at the interface (Figure 8b bottom). Figure 8c also shows the atomic density profiles of oxygen atoms of water molecules as well as saturated and unsaturated carbon atoms of POG acyl chains along Δz . The 100 times scaled atomic density profiles of the C_α carbon of Cys₈, Trp₉, Cys₁₁, and Met₂₁ residues are also shown in Figure 8c. The density profiles show a good agreement with the hydrophobicity index. In practice, a low water density is found around Trp₉, which is consistent with the formation of NFKyn via direct ozonolysis. The water density around Met₂₁ is observed to be sufficiently high to expect secondary ROS formation and subsequent reaction to yield MetSO. In contrast, the low water density near Cys₈ and Cys₁₁ inhibits formation of secondary ROS that would lead to their oxidation.

Based on the competitive reactivity of POG and SP-B₁₋₂₅ with O₃ we suggest above that they are co-located at the interface. The MD simulations of SP-B₁₋₂₅ in a lipid monolayer support our interpretation. Trp₉ and Met₂₁ of SP-B₁₋₂₅ lie below (in the z-direction) the location of the lipid double bonds (Figure 8c). Figure 9a shows the xy-projected density profiles of alkyl groups of lipids with the averaged positions of C_α carbons of AA residues of SP-B₁₋₂₅.

Consistent with our observation of the competitive interfacial reactivity of POG and SP-B₁₋₂₅, it is noteworthy that lipid acyl chains do not shelter the peptide at the air-liquid interface. The top view of the MD simulation final snapshot in Figure 9b illustrates that SP-B₁₋₂₅ is not shielded by unsaturated carbons (black spheres) of lipids. The strong amphiphilic characteristic and the large surface area of SP-B₁₋₂₅ cause the peptide to position itself at the air-liquid interface where it displaces lipids. As a result, SP-B₁₋₂₅ forms an island in a lipid monolayer that causes the hydrophobic portion of the peptide to be exposed to O₃ despite its location below the position of lipid double bonds. We also simulated SP-B₁₋₂₅ in the POPG monolayer, which is a representative anionic unsaturated phospholipids in PS.⁵⁴ The POPG monolayer exhibit almost identical atomic density profiles compared to POG monolayer with 60 Å²/lipid surface density (Figure S3 in Supporting Information). Slightly stronger interaction between POPG and water is observed from their larger area of overlapping density (~1.6 times). This is due to the strong ion-dipole interactions between POPG phosphate group and water molecules, which is absent from the POG monolayer. The peptide penetrates deeper into the POPG monolayer due to the strong electrostatic interaction between the cationic AA residues (Arg₁₂, Arg₁₇, and Lys₁₆) and the anionic phosphate group of POPG (Figures S4a and S4b in Supporting Information), which agrees with previous simulations in anionic lipid monolayers.^{50,55} SP-B₁₋₂₅ forms an island in the POPG monolayer and the anhydrous environment in the lipid monolayer renders SP-B₁₋₂₅ more susceptible to direct ozonolysis than to modification by secondary ROS (Figures S4c and S5 in Supporting Information).

Conclusions

Summarizing, to understand the unique chemistry of a surfactant protein at a model lung surfactant/air interface under O₃ exposure, we utilized the unique sampling capability of the FIDI-MS technique to examine chemical reactions in this boundary region. In the FIDI-MS spectra, oxidized products distinct from those formed in the solution phase were observed from SP-B₁₋₂₅ alone and imbedded in the POG monolayer. We also carried out MD simulations that provide additional insights into the interactions between lipids, SP-B₁₋₂₅, and water molecules in the interfacial region. In these simulations the location of SP-B₁₋₂₅ relative to the lipids provides a rationalization for the experimental observation that the peptide competes with the lipids for reaction with O₃.

Possible protection of SP-B from homogeneous oxidation by PS lipids has been suggested in an earlier study¹³. However, we have shown that SP-B₁₋₂₅ is oxidized directly by heterogeneous reaction with O₃ since it is located at the air-liquid interface with significant exposure to O₃. The solution phase oxidation of SP-B by secondary ROS is known to reduce its surface activity and function.^{13,15} We have observed fast formation of NFKyn from the direct ozonolysis of Trp₉ at the hydrophobic N-terminal side of SP-B₁₋₂₅. Our data are consistent with a model in which the oxidized residue reduces the hydrophobicity of the N-terminal side of SP-B₁₋₂₅, facilitating migration of the peptide from the interfacial region to the liquid phase. This would result in NFKyn, Cys₈, and Cys₁₁ being further oxidized by exposure to secondary ROS. In separate studies we have also examined the heterogeneous ozonolysis of a mixture of saturated and unsaturated phospholipids at the air-liquid interface using FIDI-MS. Only the unsaturated lipid reacts with ozone, forming products that are more water soluble. With extensive ozonolysis only the saturated lipid remains at the droplet surface.⁵⁶

Our findings present a detailed explanation for the mechanisms of the possible damage to the pulmonary surfactant protein SP-B by secondary ROS or direct ozone exposure. Further studies with a more elaborate model system comprising SP-B, SP-C, and various lipids could further clarify the effect of other environmental exposures, such as smoking and airborne particles, on our lung surfactant system.

Supplementary Material

Refer to Web version on PubMed Central for supplementary material.

Acknowledgments

The research described in this paper was carried out at the Beckman Institute and the Noyes Laboratory of Chemical Physics at the California Institute of Technology, the Computational NanoBio Technology Laboratory at Georgia Institute of Technology, and Jet Propulsion Laboratory under a contract with the National Aeronautics and Space Administration and funded through the Director's Research and Development Fund. We gratefully acknowledge financial support provided by National Science Foundation (NSF) under grant No. CHE-0416381 (JLB, PI) and the Beckman Institute Mass Spectrometry Resource Center. YSS and JRH acknowledge the support of the National Cancer Institute under grant No. 5U54 CA119347 (JRH, PI).

References

1. Jerrett M, Burnett RT, Pope CA, Ito K, Thurston G, Krewski D, Shi YL, Calle E, Thun M. *N Engl J Med* 2009;360:1085–1095. [PubMed: 19279340]
2. Anseth J, Goffin A, Fuller G, Ghio A, Kao P, Upadhyay D. *Am J Respir Cell Mol Biol* 2005;33:161–168. [PubMed: 15860796]
3. Halliwell B, Gutteridge J. *Biochem J* 1984;219:1–14. [PubMed: 6326753]
4. Stansfield, A.; Jump, Z.; Sodlosky, S.; Rappaport, S.; Edelman, N.; Haldorsen, J.; Javed, T.; Martin, C.; Margulies, E. Lung disease data. American Lung Association National Headquarters; 2008.
5. Vangolde L, Batenburg J, Robertson B. *Physiol Rev* 1988;68:374–455. [PubMed: 3282243]
6. Schram V, Hall S. *Biophys J* 2004;86:3734–3743. [PubMed: 15189869]
7. Hawco M, Davis P, Keough K. *J Appl Physiol* 1981;51:509–515. [PubMed: 6894918]
8. Perez-Gil J, Keough K. *Biochim Biophys Acta-Mol Basis Dis* 1998;1408:203–217.
9. Longo ML, Bisagno AM, Zasadzinski JAN, Bruni R, Waring AJ. *Science* 1993;261:453–456. [PubMed: 8332910]
10. Clark J, Wert S, Bachurski C, Stahlman M, Stripp B, Weaver T, Whitsett J. *Proc Natl Acad Sci U S A* 1995;92:7794–7798. [PubMed: 7644495]
11. Pryor W, Das B, Church D. *Chem Res Toxicol* 1991;4:341–348. [PubMed: 1912318]
12. Uppu RM, Cueto R, Squadrito GL, Pryor WA. *Arch Biochem Biophys* 1995;319:257–266. [PubMed: 7771793]
13. Manzanares D, Rodriguez-Capote K, Liu SY, Haines T, Ramos Y, Zhao L, Doherty-Kirby A, Lajoie G, Possmayer F. *Biochemistry* 2007;46:5604–5615. [PubMed: 17425286]
14. Andersson S, Kheiter A, Merritt TA. *Lung* 1999;177:179–189. [PubMed: 10192765]
15. Rodriguez-Capote K, Manzanares D, Haines T, Possmayer F. *Biophys J* 2006;90:2808–2821. [PubMed: 16443649]
16. Grimm RL, Hodyss R, Beauchamp JL. *Anal Chem* 2006;78:3800–3806. [PubMed: 16737240]
17. Thornberry T, Abbatt JPD. *Phys Chem Chem Phys* 2004;6:84–93.
18. Enami S, Vecitis CD, Cheng J, Hoffmann MR, Colussi AJ. *Chem Phys Lett* 2008;455:316–320.
19. Davis EJ, Aardahl CL, Widmann JF. *J Dispersion Sci Technol* 1998;19:293–309.
20. Buehler MF, Davis EJ. *Colloid Surf A-Physicochem Eng Asp* 1993;79:137–149.
21. Voss LF, Hadad CM, Allen HC. *J Phys Chem B* 2006;110:19487–19490. [PubMed: 17004809]
22. Van Loon LL, Allen HC. *J Phys Chem A* 2008;112:7873–7880. [PubMed: 18671375]
23. Gonzalez-Labrada E, Schmidt R, DeWolf CE. *Chem Commun* 2006:2471–2473.
24. Gonzalez-Labrada E, Schmidt R, DeWolf CE. *Phys Chem Chem Phys* 2007;9:5814–5821. [PubMed: 19462577]
25. Mundy CJ, Kuo IFW. *Chem Rev* 2006;106:1282–1304. [PubMed: 16608181]
26. Chang TM, Dang LX. *Chem Rev* 2006;106:1305–1322. [PubMed: 16608182]
27. Enami S, Hoffmann MR, Colussi AJ. *Proc Natl Acad Sci U S A* 2008;105:7365–7369. [PubMed: 18487455]

28. Enami S, Hoffmann MR, Colussi AJ. *J Phys Chem B* 2008;112:4153–4156. [PubMed: 18324812]
29. Grimm RL, Beauchamp JL. *J Phys Chem B* 2003;107:14161–14163.
30. Grimm RL, Beauchamp JL. *J Phys Chem B* 2005;109:8244–8250. [PubMed: 16851963]
31. Takamoto DY, Lipp MM, von Nahmen A, Lee KYC, Waring AJ, Zasadzinski JA. *Biophys J* 2001;81:153–169. [PubMed: 11423403]
32. Bruni R, Taeusch HW, Waring AJ. *Proc Natl Acad Sci U S A* 1991;88:7451–7455. [PubMed: 1871144]
33. Gordon LM, Lee KYC, Lipp MM, Zasadzinski JA, Walther FJ, Sherman MA, Waring AJ. *J Pept Res* 2000;55:330–347. [PubMed: 10798379]
34. Roepstorff P, Fohlman J. *Biomed Mass Spectrom* 1984;11:601–601. [PubMed: 6525415]
35. MacKerell AD, et al. *J Phys Chem B* 1998;102:3586–3616.
36. Plimpton S. *J Comput Phys* 1995;117:1–19.
37. Hockney, RW.; Eastwood, JW. *Computer simulation using particles*. McGraw-Hill; New York: 1981.
38. Clauser KR, Hall SC, Smith DM, Webb JW, Andrews LE, Tran HM, Epstein LB, Burlingame AL. *Proc Natl Acad Sci U S A* 1995;92:5072–5076. [PubMed: 7761450]
39. Qin J, Chait BT. *Anal Chem* 1997;69:4002–4009. [PubMed: 9322437]
40. Seinfeld, JH.; Pandis, SN. *Atmospheric Chemistry and Physics: From Air Pollution to Climate Change*. John Wiley & Sons; New York: 1998.
41. von Gunten U. *Water Res* 2003;37:1443–1467. [PubMed: 12600374]
42. Pryor WA. *Free Radic Biol Med* 1994;17:451–465. [PubMed: 7835752]
43. Pryor WA, Uppu RM. *J Biol Chem* 1993;268:3120–3126. [PubMed: 7679107]
44. Schoneich C. *BBA-Proteins Proteomics* 2005;1703:111–119.
45. Pryor WA, Giamalva DH, Church DF. *J Am Chem Soc* 1984;106:7094–7100.
46. Berlett BS, Stadtman ER. *J Biol Chem* 1997;272:20313–20316. [PubMed: 9252331]
47. Buxton GV, Greenstock CL, Helman WP, Ross AB. *J Phys Chem Ref Data* 1988;17:513–886.
48. Karagulian F, Lea AS, Dilbeck CW, Finlayson-Pitts BJ. *Phys Chem Chem Phys* 2008;10:528–541. [PubMed: 18183314]
49. Vieceli J, Ma OL, Tobias DJ. *J Phys Chem A* 2004;108:5806–5814.
50. Kaznessis YN, Kim S, Larson RG. *J Mol Biol* 2002;322:569–582. [PubMed: 12225750]
51. Baoukina S, Monticelli L, Risselada HJ, Marrink SJ, Tieleman DP. *Proc Natl Acad Sci U S A* 2008;105:10803–10808. [PubMed: 18669655]
52. Kaznessis YN, Kim ST, Larson RG. *Biophys J* 2002;82:1731–1742. [PubMed: 11916834]
53. Kawashima S, Ogata H, Kanehisa M. 1999;27:368–369.
54. Yu S, Harding PGR, Smith N, Possmayer F. *Lipids* 1983;18:522–529. [PubMed: 6688646]
55. Freitas JA, Choi Y, Tobias DJ. *Biophys J* 2003;84:2169–2180. [PubMed: 12668426]
56. Kim, H. PhD Thesis. California Institute of Technology; 2009.

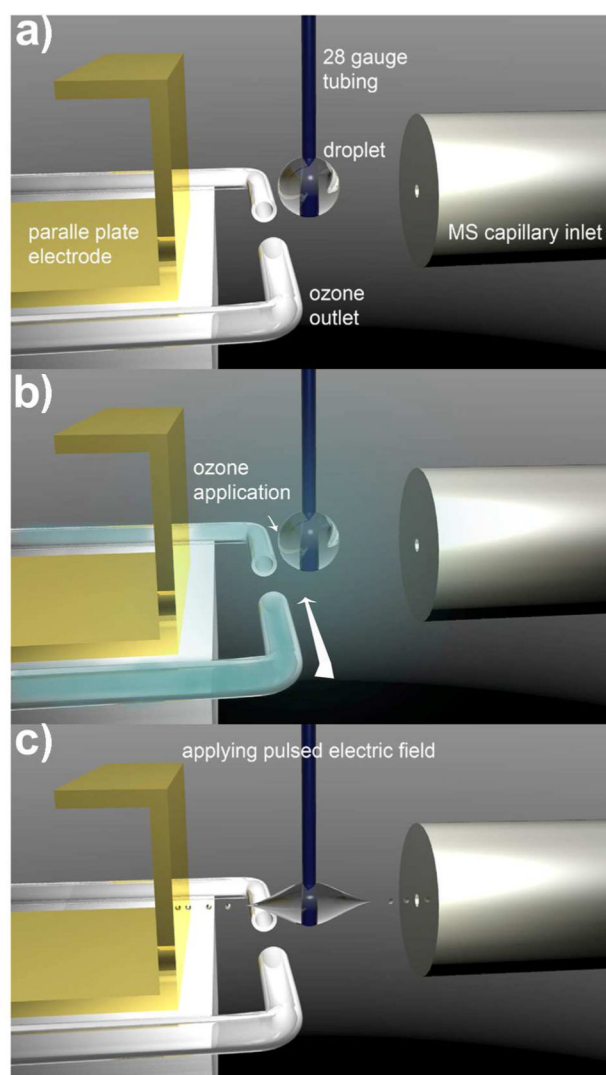


Figure 1.

Schematic illustration of FIDI-MS methodology for studies of interfacial chemistry. (a) A quiescent hanging droplet of analyte-containing solution is formed on the end of a capillary. All electrical components remain at ground as the droplet grows and reacts in a field-free environment. (b) The droplet is exposed to gas-phase reactants for a variable period of time during which heterogeneous reactions occur between the gas-phase and solution-phase species. (c) After a suitable period of reaction, a pulsed electric field stretches the neutral droplet until it emits streams of positively and negatively charged submicron droplets in opposite directions. Ionic species present in the interfacial region are sampled through the capillary inlet of the mass analyzer.

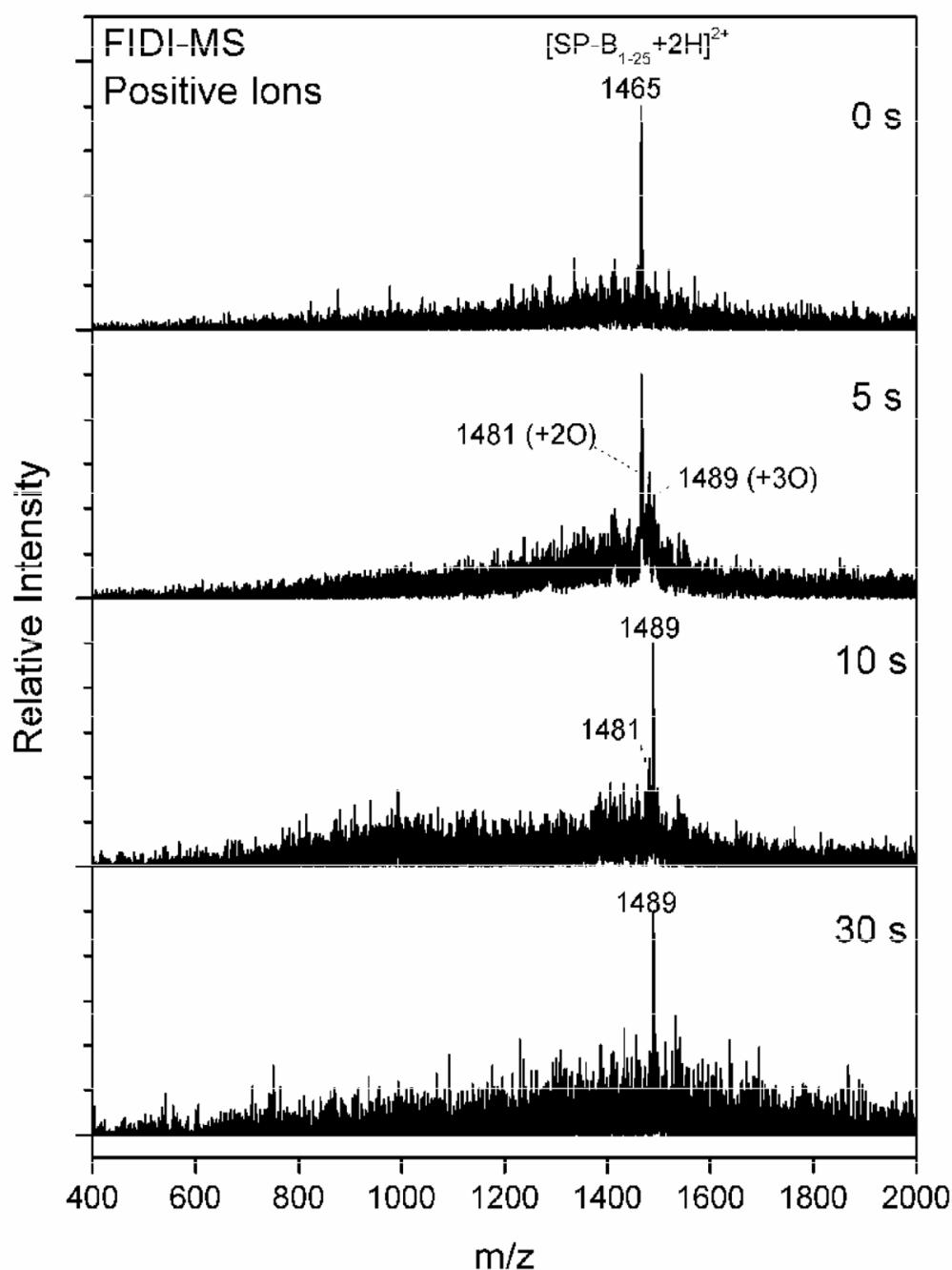


Figure 2.

(a) Air-liquid interfacial oxidation of SP-B₁₋₂₅ by O₃ as a function of time. In the absence of ozone, the positive ion FIDI-MS spectrum of SP-B₁₋₂₅ is dominated by the doubly protonated SP-B₁₋₂₅ peak at m/z 1465. The products at m/z 1481 and m/z 1489, corresponding to doubly protonated SP-B₁₋₂₅ with two oxygen atoms and three oxygen atoms, respectively, appear after the droplet is exposed to O₃ for 5 s. The triply oxygenated product at m/z 1489 dominates the FIDI-MS spectrum after exposing the droplet to O₃ for 10 s. No further oxidation of the peptide is observed up to 30 s of exposure.

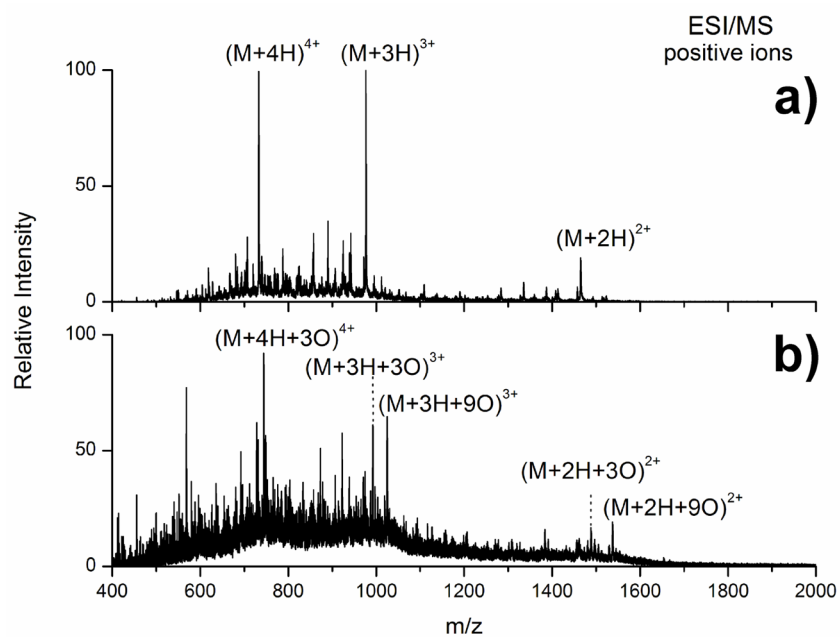


Figure 3.

(a) ESI-MS spectrum of SP-B₁₋₂₅. (b) ESI-MS spectrum of the oxidized products of SP-B₁₋₂₅ from 3 minute solution phase O₃ reaction.

SP-B₁₋₂₅: F₁P₁I₁P₂L₃P₄Y₅C₆W₇L₈C₉R₁₀A₁₁L₁₂I₁₃K₁₄R₁₅I₁₆Q₁₇A₁₈M₁₉I₂₀P₂₁K₂₂G₂₃

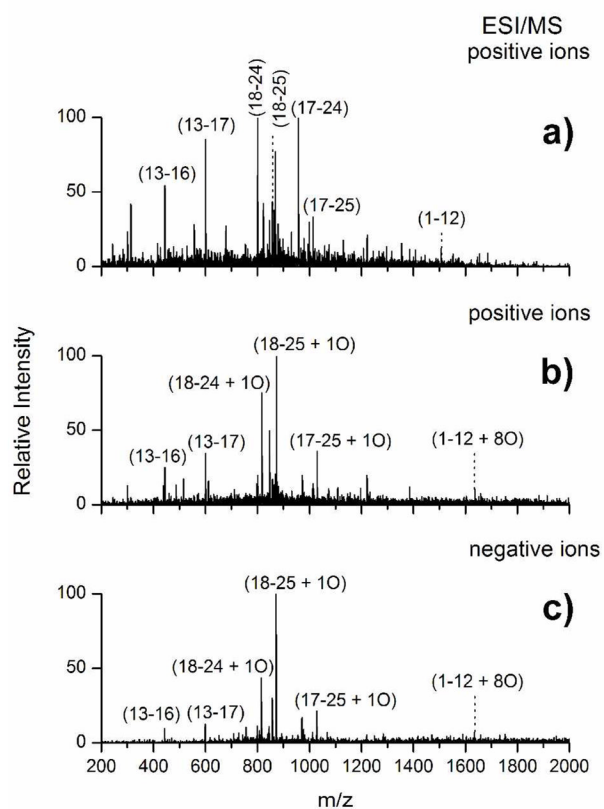
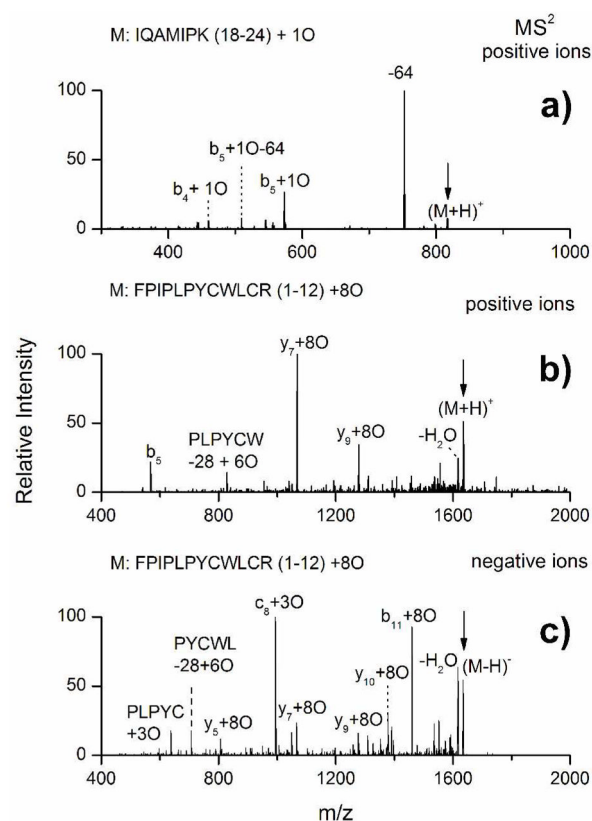
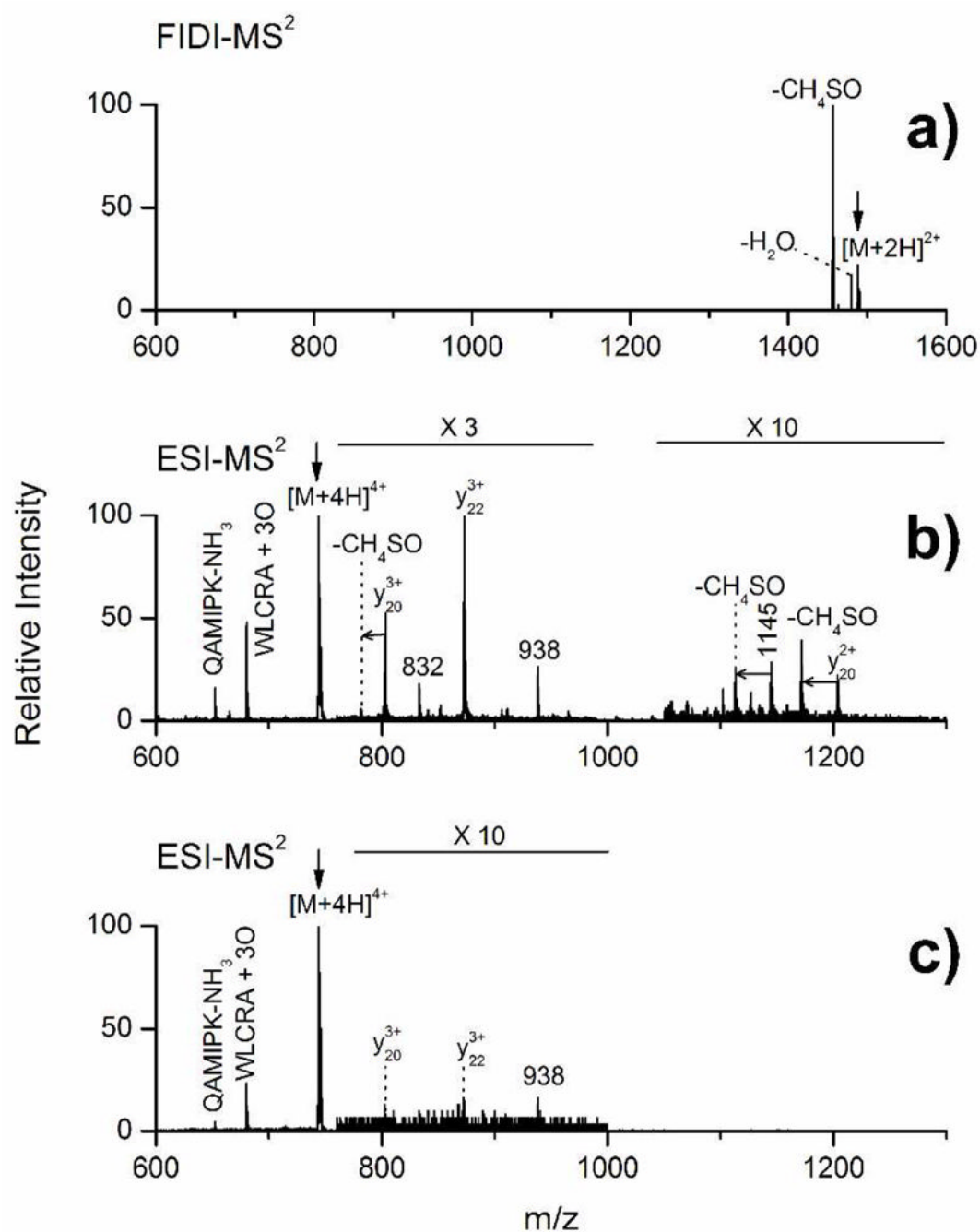


Figure 4.

(a) Positive ion ESI mass spectrum of the trypsin digest of SP-B₁₋₂₅. (b) Positive ion ESI mass spectrum of the trypsin digest of the oxidized SP-B₁₋₂₅ from the 3 minute solution phase O₃ reaction. (c) Negative ion ESI mass spectrum of the trypsin digest of oxidized SP-B₁₋₂₅ from the 3 minute solution phase O₃ reaction.

**Figure 5.**

(a) CID spectrum of cationic IQAMIPK + 3O at m/z 817 from the tryptic digest of oxidized SP-B₁₋₂₅. (b) CID of cationic FPIPLPYCWLCR + 8O at m/z 1636 from the tryptic digest of oxidized SP-B₁₋₂₅. (c) CID of anionic FPIPLPYCWLCR + 8O at m/z 1634 from the tryptic digest of oxidized SP-B₁₋₂₅.

**Figure 6.**

(a) FIDI-MS² spectrum of triply oxygenated products of doubly protonated SP-B₁₋₂₅ from heterogeneous ozonolysis. (b) ESI-MS² spectrum of triply oxygenated quadruply protonated SP-B₁₋₂₅ from solution phase O_3 reaction. (c) ESI-MS² spectrum of triply oxygenated quadruply protonated SP-B₁₋₂₅ from the Fenton reaction. M denotes a parent ion, which is triply oxygenated SP-B₁₋₂₅.

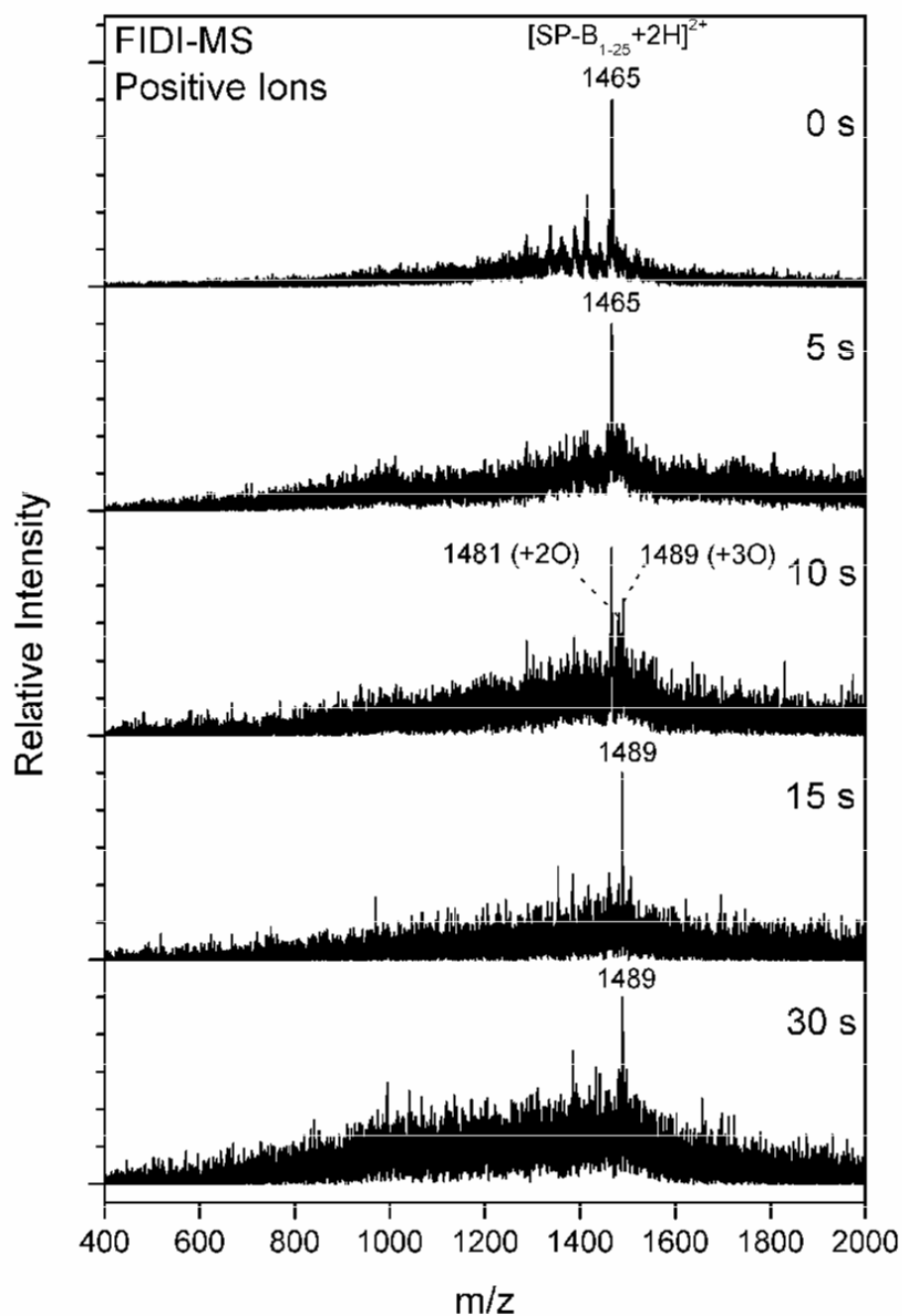


Figure 7.

Air-liquid interfacial oxidation of SP-B₁₋₂₅ by O₃ in the POG monolayer as a function of time. Doubly protonated SP-B₁₋₂₅ products with two oxygen atoms and with three oxygen atoms appear after the droplet is exposed to O₃ for 10 s. The triply oxygenated product dominates the FIDI-MS spectrum after exposing the droplet to O₃ for 15 s and no further oxidation of the peptide is observed up to 30 s of exposure.

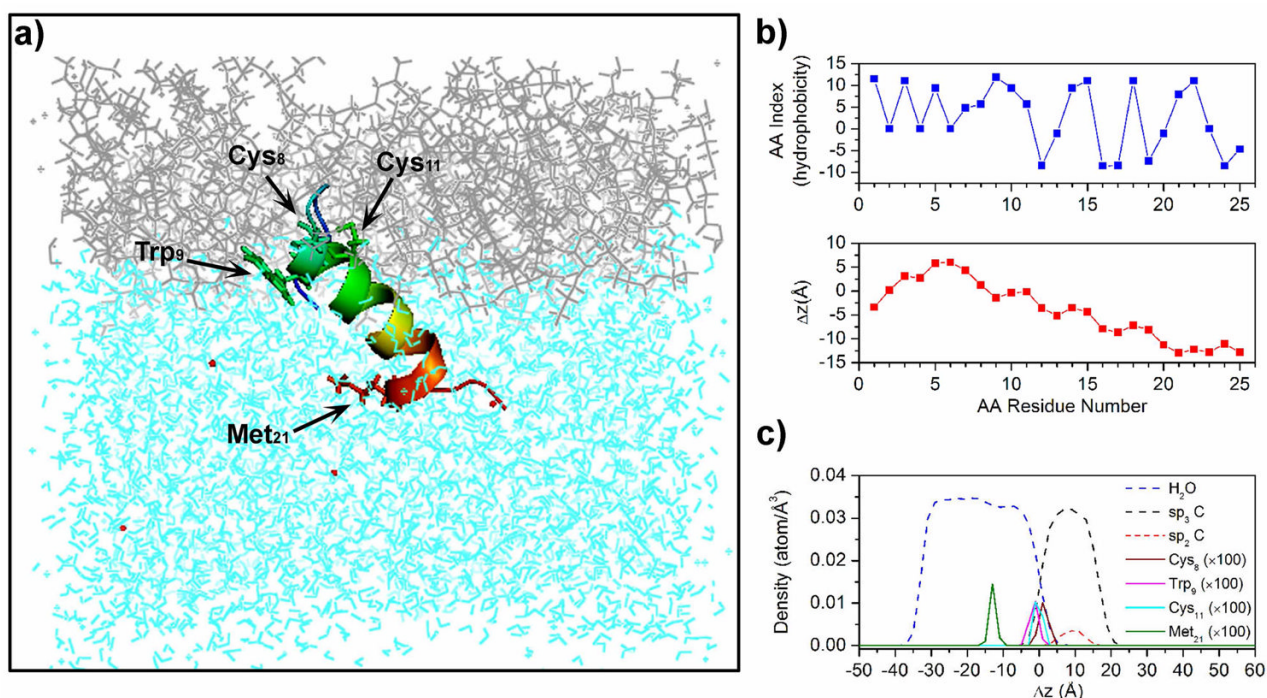


Figure 8.

(a) Final snapshot after 2.0 ns of MD simulation of SP-B₁₋₂₅ in a POG monolayer at 60 Å²/lipid. The peptide is shown in rainbow color (C-terminal: red, N-terminal: blue). Lipids, water molecules, and chloride are shown in purple, cyan, and red, respectively. (b) AA index for hydrophobicity scale⁵³ (top) and Δz of C $_{\alpha}$ of each residue averaged during the last 0.5 ns trajectory of 2.0 ns duration MD simulations (bottom) are plotted as a function of amino acid residue number. The air/water interface is located near $\Delta z = 0$. (c) Atomic density profiles of SP-B₁₋₂₅ in POG monolayer at 60 Å²/lipid as a function of Δz during the last 0.5 ns of the 2.0 ns MD simulation. Blue dash line denotes the density profiles of oxygen atoms of water molecules. Black and red dash lines denote those of saturated and unsaturated carbons of lipid acyl chains, respectively. Wine, magenta, cyan, and olive solid lines denote the 100 times scaled density profiles of the C $_{\alpha}$ carbon of Cys₈, Trp₉, Cys₁₁, Met₂₁ residues, respectively.

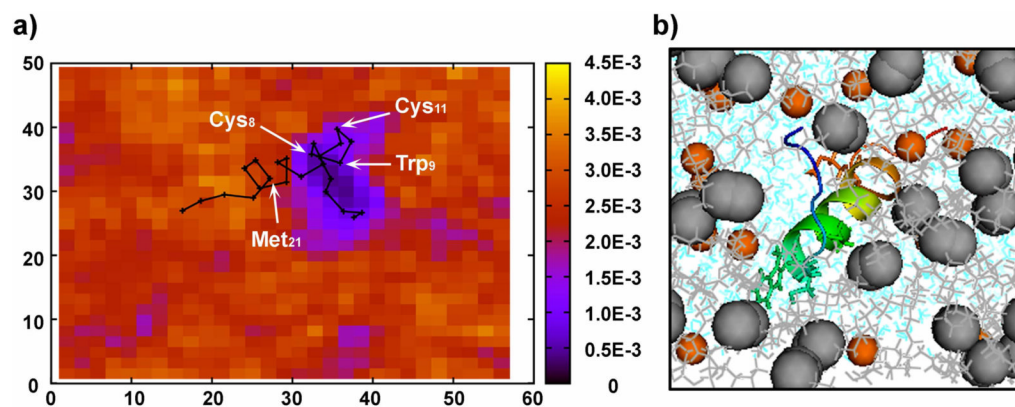
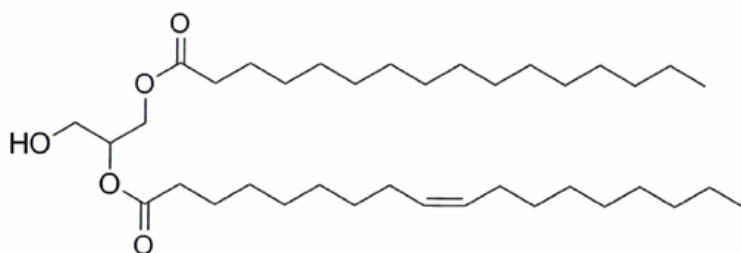
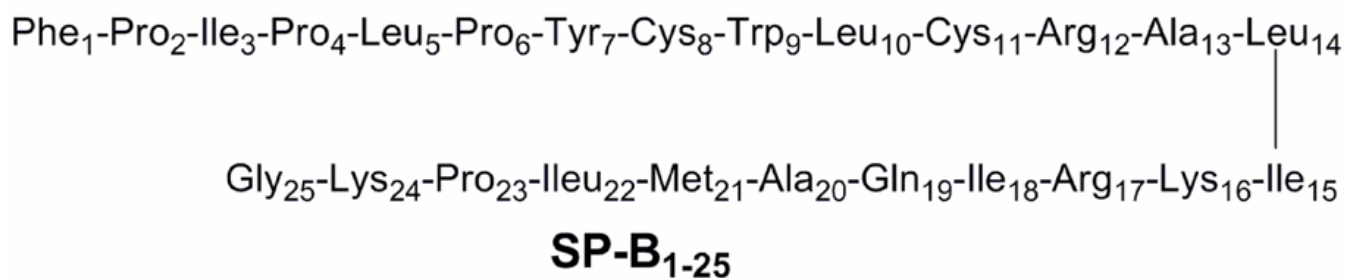


Figure 9.

(a) The xy-projected density profiles of saturated carbon atoms of lipid acyl chains from MD simulations is shown with colors and the averaged positions of C_{α} carbons of SP-B₁₋₂₅ in the POG monolayer is shown with a black line (each residue is shown with cross). (b) Top view of final snapshot after 2.0 ns of MD simulation of SP-B₁₋₂₅ in a POG monolayer at 60 Å²/lipid. The peptide is shown in rainbow color (C-terminal: red, N-terminal: blue). Lipids and water molecules are shown in gray and cyan, respectively. Black spheres denote unsaturated carbon atoms of lipid acyl chains, and orange spheres denote hydroxyl oxygen atoms.

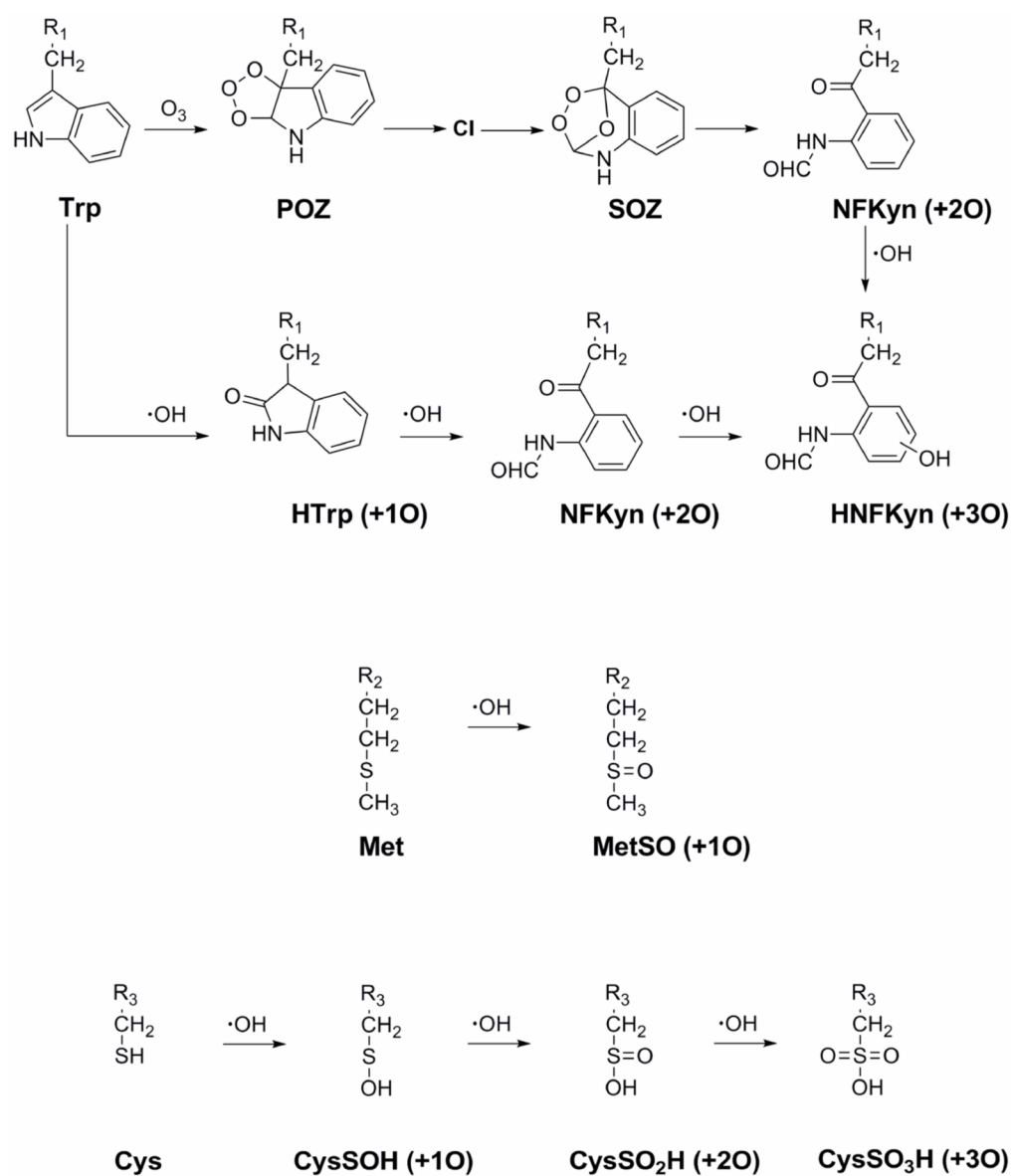


**1-Palmitoyl-2-oleoyl-*sn*-glycerol
(POG)**



Scheme 1.

Structures of POG and SP-B₁₋₂₅ investigated in this study.

**Scheme 2.**

The oxidation mechanisms of Trp, Met, and Cys in peptides by reactive oxygen species.